PAPER

Electrochemical stability of binary TiNb for biomedical applications

Materials Research Express

PAPER

Electrochemical stability of binary TiNb for biomedical applications

RECEIVED
27 November 2016

REVISED
10 April 2017

ACCEPTED FOR PUBLICATION
24 April 2017

PUBLISHED
19 July 2017

K M Reyes[1], N K Kuromoto[2], A P R Alves Claro[3] and C E B Marino[4]

[1] Laboratory of Biomaterials and Electrochemistry, Federal University of Paraná, UFPR, PR, Brazil
[2] Physics Department, Laboratory of Surface Mechanical Properties, Federal University of Paraná, UFPR, PR, Brazil
[3] UNESP—School of Engineering, Materials and Technology Department, Guaratinguetá Campus, Guaratinguetá, Brazil
[4] Department of Mechanical Engineering, Laboratory of Biomaterials and Electrochemistry, Federal University of Paraná, UFPR, PR, Brazil

E-mail: kareleiva@gmail.com **(K M Reyes)**

Keywords: Ti–Nb alloys, corrosion resistance, electrochemical stability

Abstract

The Ti–Nb alloy binary system has been widely studied with regard to biomedical applications due to the high biocompatibility and excellent mechanical properties of the alloys. Regarding physical-chemical stability, Ti–Nb alloys maintain the properties of Ti metal, which is highly resistant to corrosion in aggressive media due to a spontaneous stable oxide layer (TiO_2) formed on its surface. The objective of this study was to evaluate the corrosion resistance of the Ti–40Nb alloy in artificial blood. The thermodynamic stability was studied using the open circuit potential technique and the corrosion resistance was assessed by potentiodynamic measurements and electrochemical impedance spectroscopy. The electrochemical results indicated that the Ti–40Nb alloy has high corrosion resistance and good thermodynamic stability, with an OCP of around -485 mV, and the alloy remained electrochemically stable in potentiodynamic conditions with initial and final potentials of -1.0 V to $+2.0$ Vsce, respectively, in low current densities ($\sim\mu$A cm^{-2}) with an absence of hysteresis, aspure Ti. The results obtained showed that this specific alloy has the potential to be used in biomedical applications.

Introduction

Metals used for biomedical applications must have specific properties depending on the required functions. The principal property is biocompatibility, followed by corrosion resistance and mechanical compatibility. Thus, due to their high corrosion resistance in biological media, the principal metallic biomaterials used worldwide are pure titanium and titanium alloys [1]. Titanium has specific properties which make it an appropriate material for use in medicine, and it is proven that this element is extremely resistant to corrosion in aggressive environments (environments containing acids). This property is due to the formation of a spontaneous oxide layer of TiO_2 which is passive, very stable and biocompatible [2]. Commercially pure titanium and Ti–6Al–4V alloy are commonly used materials in odontology and orthopedics, respectively [3–5]. Several studies showed the need to develop new alloys without aluminium and vanadium, as the ions of these metals, when they are released from the Ti–6Al–4V alloy in the corrosion process, may be related to long-term health problems [6]. Scientific studies [7–9] show that the most appropriate alloying elements are niobium, tantalum, zirconium and molybdenum due to their non-toxic characteristics, the majority of these elements being β phase stabilizers [8]. Niobium was considered for use in bio implants due to it being a non-toxic, non-allergenic element [10] and for presenting high biocompatiblity [11]. Niobium also has high yield strength and ductility when compared to cortical bone [12]. Another important characteristic that makes niobium a promising material for use in biomedical applications is its stability and resistance in corrosion media [13, 14]. Currently, several researchers [15, 16] are studying the Ti–Nb alloys for presenting a low elastic modulus compared to titanium and Ti–6Al–4V orthopedic alloy, which is a very important property to reduce the stress shielding. When the bone tissue and the implant surface are undergoing the same strain, the 'stress shielding' phenomenon may be caused by the big difference in the elastic modulus of these materials. As a consequence, bone resorption can occur and then the loss of the implant in the long term. Ti–Nb alloys have been studied for showing high corrosion resistance in physiological media and for being low cost alloys

Table 1. Element percentages in the Ti–40Nb alloy obtained by x-ray fluorescence.

Element	Percentage (%)	Variation (%)
Ti	57.902	±2
Nb	42.091	±2

with the potential to be used as the Ti–6Al–4V orthopedic alloy [17, 18]. The following research aims to analyze the corrosion resistance and electrochemical stability of the commercially pure materials titanium, niobium and the biomedical Ti–40Nb alloy in media containing chloride ions using electrochemical techniques.

Experimental procedure

Samples of commercially pure titanium (grade 2) (99.35%+) were provided by Titanium do Brasil Ldta and commercially pure niobium samples (99.8%) were provided by Companhia Brasileira de Metalurgia e Mineração CBMM. The biomedical Ti–40Nb alloy was prepared at UNESP, Department of Materials, School of Engineering, Guaratinguetá Campus. In the process, the titanium and niobium materials were melted in an arc furnace under an argon atmosphere, and were remelted ten times to ensure homogeneity. After casting it underwent a homogenizing heat treatment at 950 °C for 24 h and was thencooled in the furnace. After this step, the ingot was forged by rotory swaging and then solubilization was carried out at 900 °C for 2 h, before being cooled in water. Samples with a diameter of 10 mm and a thickness of 2 mm were obtained from the cylinder ingot after wire drilling. In the preparation of the sample surface, sanding was carried out with silicon carbide sandpaper from the brand 3M, in particle sizes of 280–600. After sanding, the samples were washed in an ultrasound bath with acetone, isopropyl alcohol and distilled water (15 min in each solution). The chemically etched samples were analyzed using a microscope (Olympus FV10i) with ultraviolet laser light. The samples were sanded and then polished in an alumina 1.0 μm suspension. The material's crystalline phases were identified using an x-ray diffractometer (Shimadzu XRD-7000). The measurementswere made using CuKα monochromatic radiation with 40 kV potential and 30 mA in θ–2θ geometry, using an angle measuring 30°–90° and a scanning speed of 0.5° min^{-i}.

An electrolyte of artificial blood was used for studying the corrosive resistance and the electrochemical stability of the materials, in accordance with the ASTM F-2129. The artificial blood had the following chemical composition: NaCl 6.8 g l^{-1}, KCl 0.4 g l^{-1}, $CaCl_2 \cdot H_2O$ 0.2 g l^{-1}, $NaH_2PO_4 \cdot H_2O$ 0.026 g l^{-1}, $Na_2HPO_4 \cdot H_2O$ 0.126 g l^{-1}, $MgSO_4$ 0.1 g l^{-1}, $NaHCO_3$ 2.2 g l^{-1} with a pH of 7.3. The reference electrode used was the saturated calomel electrode (SCE), Hg/Hg_2Cl_2, KClsat and the counter electrode used was a spiral shaped platinum wire. A Minipa ET-2652 precision multimeter was used to measure the open circuit potential. A potenciostat galvanostat (Microquímica MQPG-01) was used for the cyclic voltammetry and potential linear scanning measurements. The Ei and Ef potentials were −1.0 and 2.0 V, respectively, and the scan rate was 1.0 mV s^{-a}, at room temperature. The kinetic measurements by electrochemical impedance spectroscopy were made in an electrochemical system, Ecochemie, model Autolab—PGSTAT-100, using a computer interface for the data acquisition and registry. The potential amplitude was set to 10 mV peak-to-peak (AC signal), with five points per decade, and the frequency range was set from 100 mHz to 100 kHz. The impedance tests were performed on 0, 30 and 60 d of immersion in artificial blood. For the 0 d tests, the samples stayed in the physiologic solution for 15 min until the open circuit potential was achieved.

Results and discussion

Table 1 shows the concentration of the elements titanium and niobium in the Ti–40Nb alloy. The percentage of niobium in the alloy is 42.0 ± 2% and the percentage of titanium is 57.9. ± 2%. These values are almost the quantities in bulk of the metals used in the preparation of the alloy Ti–40Nb. The x-ray analysis suggests the homogeneity of the alloy which was custom made in the laboratory.

An image of the optical microscopy of the titanium grade 2 surface after etching with specific etch for titanium (Kroll reagent) is shown in figure 1(a). A uniform microstructure of titanium CP is noted, presenting only α structure. As shown in the image, there is a uniform distribution of the grains and a minimal variation in the coloring which indicates the different crystallographic axes. The variation in the sizes of the grains revealed is approximately in the order of 10 μm minimum and 70 μm maximum [19].

Many authors suggest that the Ti–Nb alloys present different microstructures; these microstructures are sensitive to the content of niobium present in the alloys, to the thermomechanical processing, and to the cooling in the preparation and thermal treatment of the alloy [15, 20–23, 27, 28].

Following the schematic phase diagram for the titanium alloys, there are just three stable phases in the Ti–Nb binary system, however, the transformation $\beta \rightarrow \alpha$ is slow, allowing the occurrence of some metastable transformations. The β phase suffers two types of martensitic transformations while being fast cooled: α' (hexagonal)

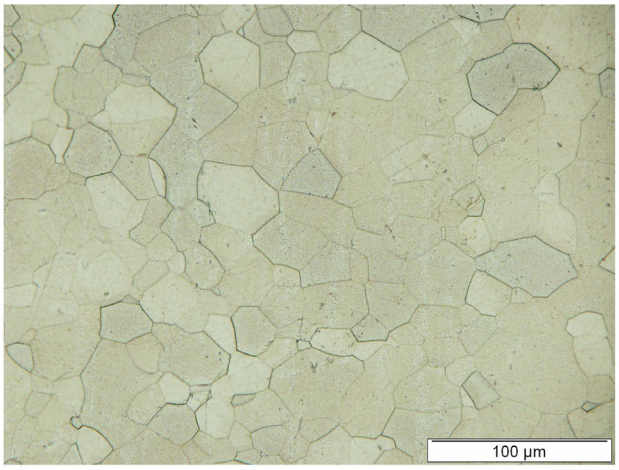

a)

b)

Figure 1. (a) Optical microscopy image of the surface of Ti CP chemically etched with Kroll reagent, (500×), (b) optical microscopy image of the Ti–40Nb alloy's surface chemically etched with a special reagent for niobium and its alloys (ASTM 160), (200×).

and α'' (orthorhombic). In small compositions, the ω hexagonal phase is caused by the instability of the β phase, due to the cooling process. It occurs when there is a transition phase between the β and α phases because of the thermal treatments [22].

Figure 1(b) shows the Ti–40Nb alloy microstructure after the process to reveal the phases and grain outline with the chemical etch. This optics micrograph suggests that the structure presented by the Ti–40Nb alloy was a biphasic structure composed by α'' *e* β phases (shown by arrows in the figure). The fast cooling, from a high temperature where there is a presence of the β phase, produces α'' and ω [24], which were probably obtained during the water cooling, after the solubilization treatment. However, by having a large amount of niobium, we obtained a fraction of the β phase retained after the fast cooling, and possibly retention of the ω phase according to data in the literature [25, 26].

Figure 1(b) suggests diverse β grains with diameters of about 70 and 100 μm. There are also denotations of grains with the structure of the martensitic phase, with an approximate diameter of between 80 and 120 μm. The structure presented is uniform in every grain, where it is possible to see that there is variation in the size of the revealed grains, in the order of 120 μm in its bigger sizes.

The crystallographic data sheet derived from the stable and metastable diagrams for the Ti–Nb alloy [29], indicate that the phases β (Ti) and β (Nb) (cubic) can be observed in the alloys that have 0–100 wt.% of Nb, the α'' (Ti) (orthorhombic) phase can be present in alloys with ~14–43 wt.% of Nb. The ω and phase α'' (hexagonal) can be present in alloys within 16–45 wt.% of Nb, depending exclusively on the alloy's preparation process.

According to previous research, biphasic alloys obtained by different cooling methods can have distinct electrochemical behavior, such as Ti–35Nb which presented $\alpha'' + \beta$ phases when processed using water cooling and $\alpha + \beta + \omega$ phases when processed using oven cooling [17]. The presence of α'' phase coexisting with β phase can also infer in the elastic modulus property by means of the presence of the β phase. Several biphasic titanium alloys are commercially used, such as the $\alpha + \beta$ alloy Ti–6Al–4V (ASTM F 1472), Ti–13Nb–13Zr and Ti–Zr, which have microstructures that are martensitic and beta phases [30].

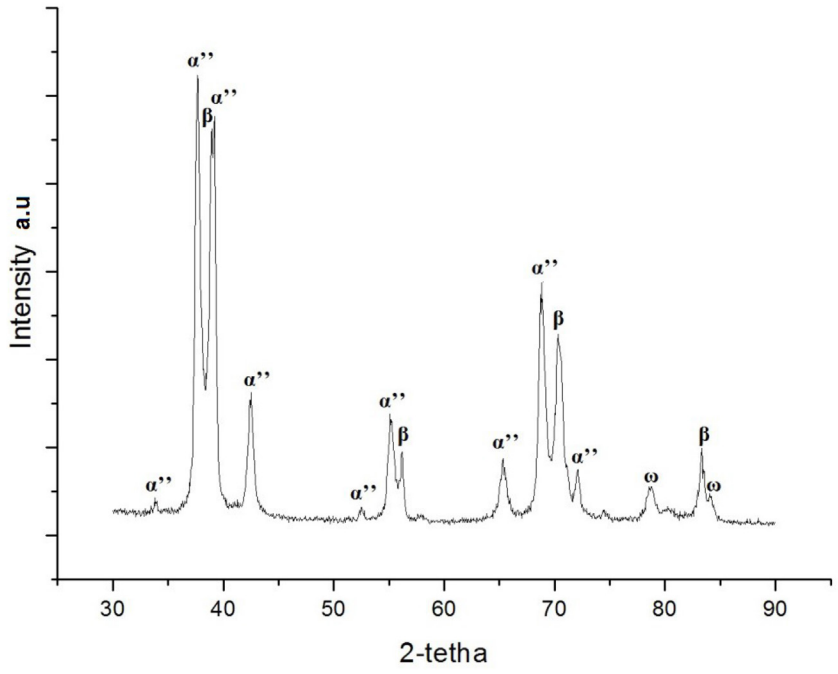

Figure 2. XRD spectra for the biomedical Ti–40Nb alloy with scanning speed of 0.5° min^{-1}.

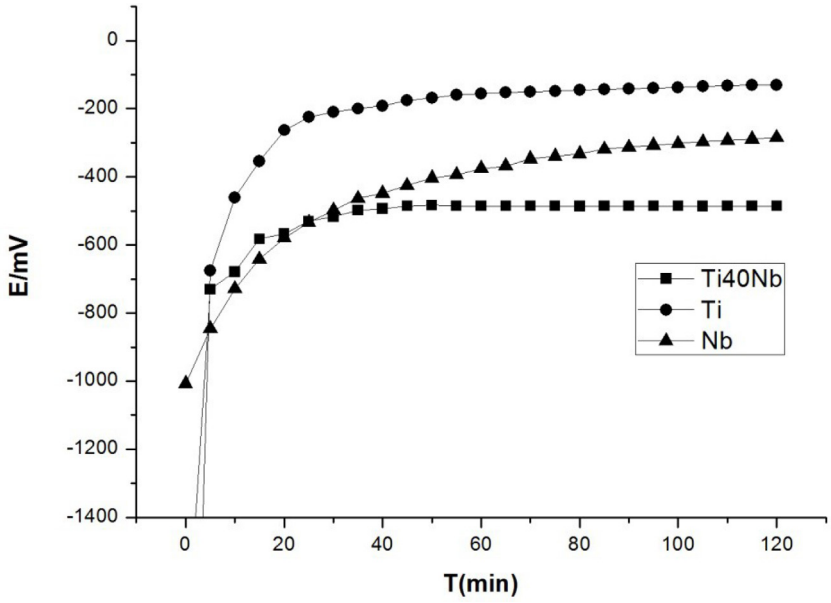

Figure 3. Open circuit potential curves of biomaterials Ti–40Nb, titanium and niobium in artificial blood at room temperature, (pH ~ 7.4).

Analyses were realized using the x-ray diffraction technique (XRD) in the samples, to prove that the ω phase was formed in the metallurgic Ti–40Nb alloy. Figure 2 shows the diffraction spectrum obtained in the XRD analyses of the Ti–40Nb alloy in the θ–2θ geometry. Fifteen peaks with different intensities are recognized, this being determined by analyses and comparison with the data bank of the 'joint committee on powder diffractions standards (JCPDS)' sheet.

As shown in figure 2, the α'', β and ω phases observed in the biomedical Ti–40Nb alloy by the microstructure analyses were also identified by XRD spectra, proving the presence of the three phases in the biomaterials samples.

Electrochemical stability and corrosion resistance

Figure 3 shows the open circuit potential (OCP) for titanium, niobium, and the Ti–40Nb alloy, respectively. For being valve metals (recovered with a spontaneous oxide) the OCP curves showed a particularly similar behaviour, where the growth of this spontaneous oxide layer is associated with a linear increment of the potential over time (figure 3). The positive potential evolution indicates the formation of a protecting passivation layer.

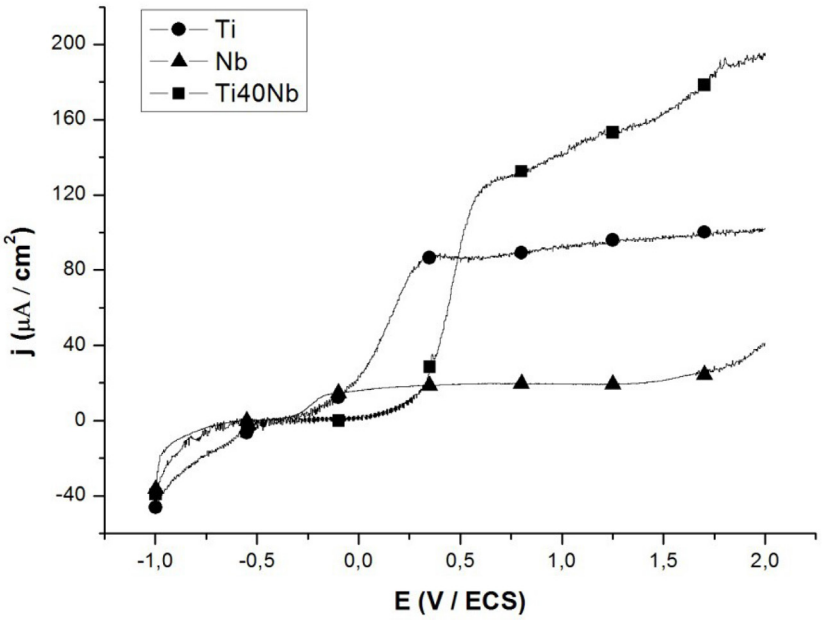

Figure 4. Potentiodynamic curves of niobium, titanium and Ti–40Nb alloy in artificial blood solution at scan rate of 1 mV s^{-1} at room temperature.

The surface activation of the material takes place from the first minute the metal is exposed to the electrolyte. The potential shifts toward more positive values in the first minutes (0–15 min), and after this time the stationary state is achieved at certain equilibrium potential (figure 3). In this condition, the surface must be covered with a spontaneous oxide layer of around 2 nm thickness [31].

In the case of titanium, the electrochemical stability is achieved in about 20 minutes, which indicates the stationary state and the presence of a TiO_2 layer on the metal surface. Titanium's equilibrium potential was approximately −131 mV, indicating that this biomaterial is stable in artificial blood. In the case of niobium, it was not possible to determine the time when the stationary state was achieved; a subtle increase in the potential with time was observed during the 120 min experiment, so the formation of a protective layer of Nb_2O_5 on the substrate can be assumed. The equilibrium potential of niobium (−284 mV) indicated that this material has a greater tendency to dissolution/corrosion in artificial blood.

The biomedical Ti–40Nb alloy presents similar behavior to that of titanium, obtaining thermodynamic stability in approximately 27 min. For the titanium based alloy, the tendency for oxide to form in artificial blood media was alike. In this case, after the 27 min of exposure, there was no variation in the potential over time. This indicates the stationary state of the alloy but it occurs in a less noble potential than in the case of niobium, being −485 mV, which indicates that this alloy is thermodynamically less stable.

A less noble OCP in the alloy could be obtained because of the cooling process employed in the preparation of the alloy, which produces α'' phase [17] and causes less corrosion resistance [32]. Thermodynamical stability of Ti–40Nb alloy in artificial blood can be compared to the commercial Ti–6Al–4V alloy, for which the OCP' is around −500 mV [31, 33].

The potential linear scanning method was used to study the electrochemical stability of materials under controlled potential conditions. Figure 4 shows the potentiodynamic polarization curves and the current density values obtained at a scan rate of 1 mV s^{-1}, in artificial blood solution for titanium, niobium and Ti–40Nb.

As seen in figure 4, in both biomaterials (Ti and Nb) when anodically polarized, a protective oxide grew, which is inferred from the increase in the charge ($I \times t$) involved in the process. In the case of niobium, there was a smaller potential and smaller current density than titanium, which may indicate that the formation of Nb_2O_5 occurs faster than the formation of TiO_2. Regarding the Ti–40Nb alloy, the formation of the surface oxide occurs steadily over a current density of 140 μA cm^{-2} and a polarization potential of 0.65 V.

The three materials maintained the typical behaviour of a passive material [34, 35], no breakdown potential was observed during the applied potential range. The breakdown potential its characterized by the sudden increase in the current density in a certain potential, which indicates the passage of current through the breaking of the surface oxide layer. As no increase in the current density was observed for these biomaterials, the films formed on the surface of the biomaterials were stable and protective [36].

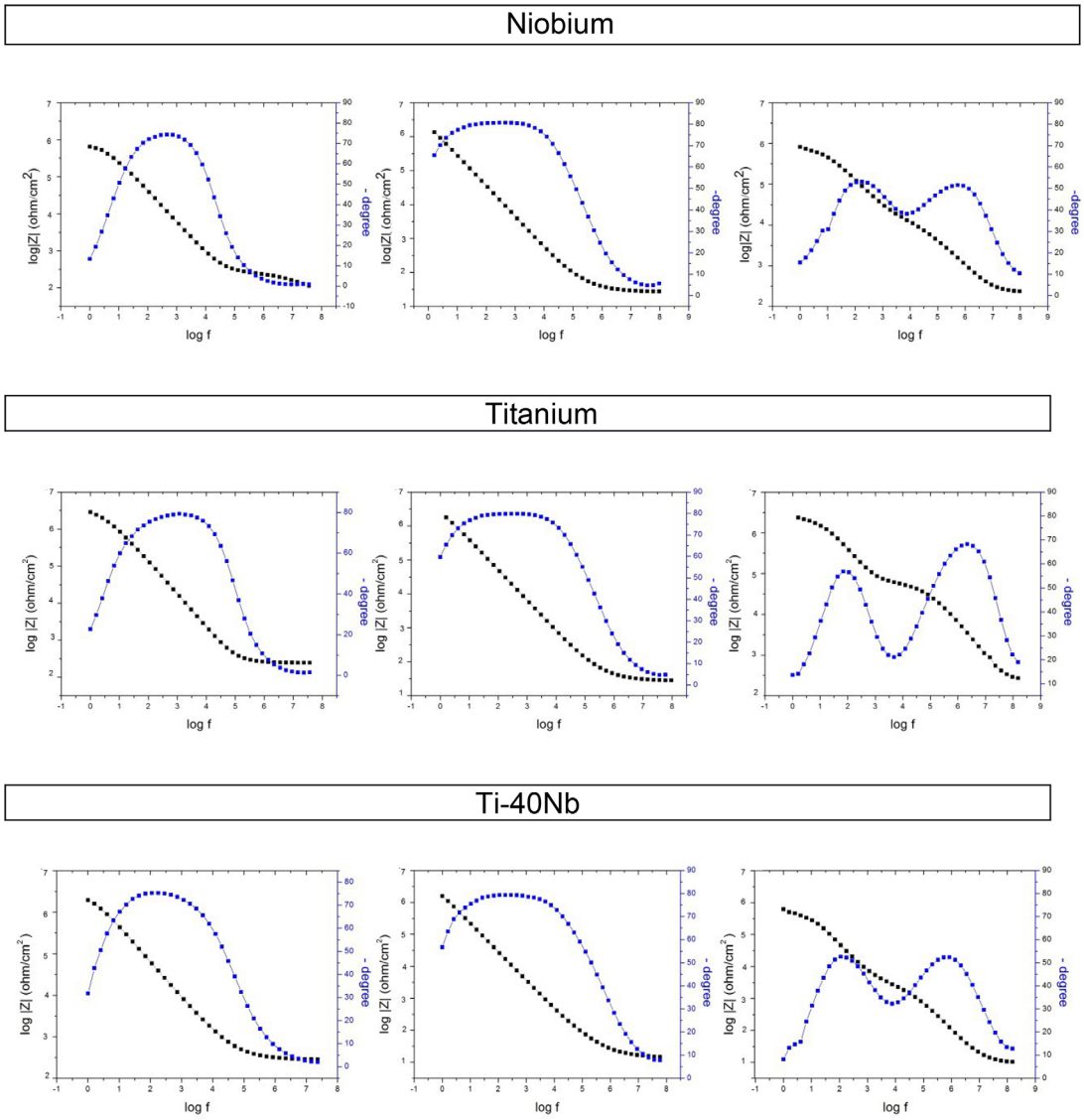

Figure 5. Bode plots of (a) niobium (b) titanium and (c) Ti–40Nb in 0, 30 and 60 d of immersion in artificial blood at room temperature, pH ~ 7.4 with an AC potential of 10 mV and DC potential of the OCP.

Thereby, by comparing the magnitudes of the peak potential presented by the biomaterials: −0.20 V for niobium, 0.30 V for titanium and 0.65 V for Ti–40Nb alloy, we can see that the formation of the barrier oxide layer occurs more rapidly for the niobium, followed by titanium and finally the Ti–40Nb alloy. Also, as shown in figure 4, the integral of the curves $j \times E$, which represents the charge (Q) involved in the anodic process, indicates quantitative characteristics of the surface oxide. Since the charge in the anodic process of the Ti–40Nb alloy was greater than the one presented in titanium, possibly there is a larger amount of this oxide on the alloy surface, which denotes a more protective behavior. As for the niobium, where the charge is less compared with the other biomaterials, there should be less oxide on the surface, demonstrating a weaker barrier system. However, there was no stabilization of the current density at the end of scan potential for Ti–40Nb, so this behavior may indicate that even if there is more of this oxide, it is a more unstable layer. Regarding the magnitude of the thickness of these oxides, Marino [32] studied the growth of titanium oxide with anodic charges, showing that the anodizing rate is 2.5 nm V^{-1}. Thus, the estimated thickness of the surface oxide on Ti–40Nb alloy should be approximately 5.0 nm.

To study the kinetics of the corrosion process in the biomaterials, the electrochemical impedance spectroscopy (EIS) technique was employed to analyze the electrical parameters of resistance and capacitance. In figure 5, Bode diagrams are shown. In these diagrams the impedance spectrum can be seen for niobium, titanium, and Ti–40Nb alloy on 0, 30 and 60 d of immersion in artificial blood. Both impedance module (Z) and phase angle (θ) are represented as a function of frequency.

The $\log|Z| \times \log f$ curve provides the $R_p + R_s$ values, where R_p is the polarization resistance at low frequencies and R_s the solution resistance at high frequencies. A superior impedance and phase angle (of around 90°), indicates a nobler electrochemical behavior because both are related to the resistance of the oxide layer [17, 37]. The electrical parameters obtained for each material are shown in table 2.

Table 2. Results of the electrical parameters obtained for (a) titanium (b) niobium and (c) Ti–40Nb at 0, 30 and 60 d of immersion in artificial blood at room temperature, pH ~ 7.4 at 10 mV AC potential and the open circuit DC potential.

Parameters	Ti	Nb	Ti–Nb	Ti	Nb	Ti–Nb	Ti	Nb	Ti–Nb
	0 d			30 d			60 d		
Phase angle	−80°	−73°	−74°	−81	−82	−79	−70°, −56°	−53°, −55°	−54°, −55°
R_s ($\Omega \cdot cm^2$)	18	17	17	12	15	14	19	17	13
R_p($M\Omega \cdot cm^2$)	2.85	0.56	1.54	2.83	0.50	1.52	2.80	0.48	1.48
C ($\mu F\ cm^{-2}$)	6.02	16.9	7.11	6.08	17.23	7.15	6.12	17.3	7.19

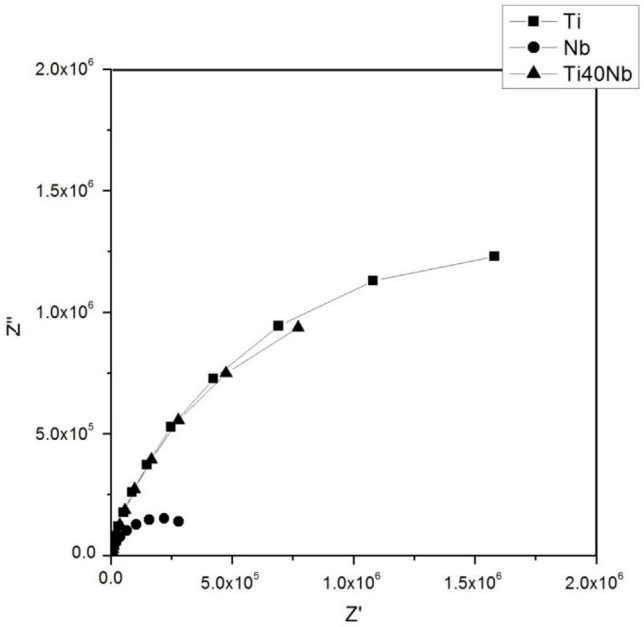

Figure 6. Nyquist plot for titanium, niobium and Ti–40Nb alloy in artificial blood at room temperature, pH ~ 7.4 with an AC potential of 10 mV and DC potential of the OCP.

The polarization resistance refers to the oxide/solution interface and, for all the biomaterials, was around 10^6, i.e. there is a very resistant oxide layer in the surface, a barrier type oxide. The lower absolute values of polarization resistance were presented by niobium, followed by Ti–40Nb and finally, titanium grade 2. With regard to the phase angle, it remained constant in the intermediate frequencies in the case of 0 and 30 d of immersion in artificial blood, which represents a capacitive behavior.

Analysing figure 5; for titanium, niobium, and the Ti–40Nb alloy at the different times of analysis there is a typical behavior of the valve metals, where there is a grown oxide film on the surface when the potential remains in the open circuit conditions. This occurs for the different times of immersion in artificial blood. This argument is based on the fact that the capacitance value in the three different times remains in the order of $\mu F\ cm^{-2}$ for all the biomaterials. The polarization resistance value for all the biomaterials (table 2) showed only a minimal decrease over time, which may be justified because an increase is expected in the thickness of the surface oxide while keeping the biomaterial in the open circuit condition in artificial blood within 30 and 60 d. By keeping considerably high impedance values, it can be confirmed that these biomaterials remained stable and resistant to corrosion due to the oxide film that had grown on its surface, which in fact did not show any indication of spontaneous dissolution. This result corroborates the results of the potential linear scanning measuring and cyclic voltammetry, where the same electrochemical behavior of these biomaterials was predicted under accelerated conditions.

Regarding phase angle, there is a small variation between the values of 0 and 30 d of immersion in artificial blood for the three biomaterials. This indicates that in 30 d these biomaterials have become more capacitive, implying the possible formation of a more porous oxide, which is a characteristic of the valve metals. This hypothesis was confirmed in the scanning carried out at 60 d of immersion, where the electrical behavior showed two time constants for titanium, niobium and for the Ti–40Nb alloy. This time constant has been interpreted as being the result of an outer surface layer of the film, according to the bi-layer oxide model [38], where the outer layer is less compact and/or porous than the inner layer [39].

Thus, by the analysis of R_p values, titanium showed superior corrosion resistance. This result supports the thermodynamic and electrochemical stability analysis, where Ti grade 2 showed the noblest behavior. Analyzing the Ti–40Nb alloy, a high value of polarization resistance of around $10^6\ \Omega \cdot cm^2$ was proved. Scientific literature presents polarization resistance values in biological media analysis of the order of around $10^3\ \Omega \cdot cm^2$ for Cr–Co alloys and some stainless steels [36]. This indicates that the Ti–40Nb alloy presents similar behavior to titanium and to commercial Ti–6Al–4V alloy [40–42].

The capacitance values (10^{-6} F cm^{-2} for titanium and Ti–40Nb alloy and, 10^{-5} F cm^{-2} for niobium), indicates that niobium is subtly more capacitive than the other biomaterials. This may have occurred due to the type of oxide that grew on its surface, which, according to the voltammetry results, is a compact oxide with a small thickness, but probably less resistive.

In the complex plane or Nyquist diagram (figure 6) the imaginary (Z'') and the real (Z') components of impedance are indicated for the selected frequency range. In this diagram, while extrapolating the semicircles to the real axis (Z'), at the low frequencies (at the right of the spectrum) the system resistance ($R_p + R_s$) is exposed and in high frequencies (at the left of the spectrum) the solution resistance value is observed. The resistance data in the complex plane diagram clearly demonstrates that the Ti–40Nb alloy had a very similar behavior to titanium. This suggests an excellent chemical and electrochemical stability, i.e. a good resistance to corrosion. Finally, this indicator proves that this alloy could be considered as a base material for orthopedic implants when compared to Ti–6Al–4V alloy which has an Rp of around $10^6\ \Omega \cdot cm^2$ in Ringers and PSB physiological solutions [32]. Moreover, the solution resistance remained at a low magnitude (~18 Ω), where the acceptable range for electrochemical impedance measurements is equal to or smaller than 50 Ω.

Conclusions

The Ti–40Nb alloy obtained in the arc furnace is a biphasic $\alpha'' + \beta$ alloy with the presence of ω phase. The results of the electrochemical tests indicated that the Ti–40Nb alloy has good thermodynamic stability, and the potential of the stationary state was around −485 mV. The alloy remains electrochemically stable at low current densities and with no hysteresis (dissolution/corrosion). This stability may be shown to be due to the presence of a spontaneous oxide layer (~5.0 nm) of TiO_2 and Nb_2O_5 growth in the surface. The kinetic data indicated that the Ti–40Nb alloy is as resistant to corrosion in artificial blood as Ti; for both biomaterials a resistance of $M\Omega \cdot cm^2$ was shown. Thus, the Ti–40Nb alloy is an electrochemically and thermodynamically stable metallic alloy which can be considered for further research as a potential material for biomedical applications. Due to the amount of niobium involved, this would be a low cost biomedical alloy.

Acknowledgments

The authors are grateful to PIPE-UFPR (Graduate Program of Engineering and Materials Science), CAPES and OEA for financial support, and Cláudia Eliana Bruno Marino would like to thank CNPq for the productivity fellowship (grant number 301434/2013-1).

References

[1] Elias N, Lima J C, Valiev R and Meyers M A 2008 Biomedical applications of titanium and its alloys *Biol. Mater. Sci.* (https://pdfs.semanticscholar.org/89ef/4a0283ac38a252be52f5c4cec5d79be5832c.pdf)
[2] Souza A K and Robin A 2003 Preparation and characterization of Ti–Ta alloys for application in corrosive media *Mater. Lett.* **57** 3010–6
[3] Majumdar P, Singh S B and Chakraborty M 2011 The role of heat treatment on microstructure and mechanical properties of Ti–13Zr–13Nb alloy for biomedical load bearing applications *J. Mech. Behav. Biomed. Mater.* **4** 1132–44
[4] Starikov V, Starikova S, Mamalis A, Lavrynenko A and Ramsden J 2007 The application of niobium and tantalum oxides for implant surface passivation *J. Biol. Phys. Chem.* 141–5
[5] Niinomi M 2008 Mechanical biocompatibilities of titanium alloys for biomedical applications *J. Mech. Behav. Biomed. Mater.* **1** 30–42
[6] Geetha M, Singh A K, Asokamani R and Gogia A K 2009 Ti based biomaterials, the ultimate choice for orthopaedic implants, a review *Prog. Mater. Sci.* **54** 397–425
[7] Alfonso J, Rivas D and Hallen J M 2007 Discussion on 'Stochastic modeling of pitting corrosion: a new model for initiation and growth of multiple pits' *Corros. Sci.* 559
[8] O'Brien B, Stinson J and Carroll W 2008 Development of a new niobium-based alloy for vascular stent applications *J. Mech. Behav. Biomed. Mater.* 303–12
[9] Niinomi M 2012 Recent metallic materials for biomedical applications *Metall. Metallic Mater. Trans.* A **33** 477–86
[10] Johansson C B, Hansson H A and Albrektsson Y 1990 Qualitative interfacial study between bone and tantalum, niobium or commercially pure titanium *Biomaterials* **11** 277–80
[11] Sanka M, Baligidad R G and Gokhale A A 2013 Effect of oxygen on microstructure and mechanical properties of niobium *Mater. Sci. Eng.* **569** 132–6
[12] Wang W and Alfantazi A 2011 An electrochemical impedance spectroscopy and polarization study of the role of crystallographic orientation on electrochemical behavior of niobium *Electrochim. Acta* 1–10
[13] Tavares A M G *et al* 2014 The addition of Si to the Ti–35Nb alloy and its effect on the corrosion resistance, when applied to biomedical materials *J. Alloys Compd.* **591** 91–9

[14] Guo Y, Georgarakis K, Yokoyama Y and Yavari A R 2013 On the mechanical properties of TiNb based alloys *J. Alloys Compd.* **571** 25–30
[15] Matlakhova L, Matlakhov A and Monteiro A 2008 Temperature effect on the elastic modulus, internal friction and related phase transformations in Ti–Nb–2%Al quenched alloys *Mater. Charact.* 1234–40
[16] Bai Y J *et al* 2012 Electrochemical corrosion behavior of Ti–24Nb–4Zr–8Sn alloy in a simulated physiological environment *Appl. Surf. Sci.* **258** 4035–40
[17] Cremasco A, Osorio W, Freire C, Garcia A and Caram R 2008 Electrochemical corrosion behavior of a Ti–35Nb alloy for medical prostheses *Electrochim. Acta* **53** 4867–74
[18] Wang Y B and Zheng Y F 2009 Corrosion behaviour and biocompatibility evaluation of low modulus Ti–16Nb shape memory alloy as potential biomaterial *Mater. Lett.* **63** 1293–5
[19] Ratner B D, Hoffman A S, Schoen F J and Lemons J L 2004 *An Introduction to Materials in Medicine* (London: Elsevier Academic Press) pp 67–137
[20] Engel I and Klingel H 1981 *An Atlas of Metal Damage* ed S Murray (Munich: Carl Hanser, Verlage) (transl. Wolf Publishing Ltd., Lonfon)
[21] Moffatt D L and Kattner U R 1988 *Metall. Trans.* 2389
[22] Collings X *et al* 1994 Metallography and microstructure *Materials Properties Handbook: Titanium Alloys* (Materials Park, OH: American Society for Metals) p 1053
[23] Bai Y J *et al* 2011 Comparative study on the corrosion behavior of Ti–Nb and TMA alloys for dental application in various artificial solutions *Mater. Sci. Eng.* C **31** 702–11
[24] Pathak A, Banumathy S, Sankarasubramanian R and Singh A R 2014 Orthorhombic martensitic phase in Ti–Nb alloys: a first principles study *Comput. Mater. Sci.* **83** 222–8
[25] Mishra A K, Davidson J K, Poggie R A, Kovacs P and Fitzgerald T J 1996 *Medical Applications of Titanium and Its Alloys* ed S A Brown and J E Lemons (West Conshohocken, PA: ASTM STP 1272) pp 96–113
[26] Zhanga S *et al* 2016 First-principles study of phase stability and elastic properties of binary Ti–*x*TM (TM = V,Cr,Nb,Mo) and ternary Ti–15TM–*y*Al alloys *Mater. Des.* **110** 80–9
[27] Lee *et al* 2002 Structure- property relationship of cast Ti–Nb alloys *J. Oral Rehabil.* 314–22
[28] Hon Y H, Wang J Y and Pan Y N 2003 Composition/phase structure and properties of titanium–niobium alloys *Mater. Trans.* 44 2384–90
[29] ASM—American Society for Metals Handbook 1990 *Alloy Phase Diagrams* vol 3
[30] Li Y *et al* 2014 New developments of Ti-based alloys for biomedical applications *Materials* **7** 1709–800
[31] Marino C E B 2001 On the stability of thin-anodic-oxide films of titanium in acid phosphoric media *Corros. Sci.* **43** 1465–76
[32] Atapour M *et al* 2011 Corrosion behavior of beta titanium alloys for biomedical applications *Mater. Sci. Eng.* C **31** 885–91
[33] Marino C E B and Mascaro L H 2011 Electrochemical tests to evaluate the stability of the anodic films on dental implants *Int. J. Electrochem.* (http://dx.doi.org/10.1590/1516-1439.201514)
[34] Assis S L, Wolynec S and Costa I 2006 Corrosion characterization of titanium alloys by electrochemical techniques *Electrochim. Acta* **51** 1815–9
[35] McMahon R E *et al* 2012 A comparative study f cytotoxicity and corrosion resistance of nickel–titanium and titanium–niobium shape memory alloys *Acta Biomater.* **8** 2863–70
[36] Yang S, Zhang D C, Wei M, Su H X, Wu W and Lin J G 2013 Effects of the Zr and Mo contents on the electrochemical corrosion behavior of Ti–22Nb alloy *Mater. Corros.* **64** 402–7
[37] Vidal C V and Muñoz A I 2008 Electrochemical characterisation of biomedical alloys for surgical implants in simulated body fluids *Corros. Sci.* **50** 1954–61
[38] Sloppy J D, Lu Z, Dickey E C and Macdonald D D 2013 Growth mechanism of anodic tantalum oxide in phosphoric acid *Electrochim. Acta* **87** 82–91
[39] Liu J *et al* 2012 Influence of incremental rate of anodizing current on roughness and electrochemical corrosion of oxide film on titanium alloy Ti–10V–2Fe–3Al *Surf. Eng.* **28** 406–11
[40] Marino C E B, Biaggio S R, Rocha-Filho C and Bocchi N 2006 Voltammetric stability of anodic films on the Ti6Al4V alloy in chloride medium *Electrochim. Acta* **51** 6580–3
[41] Fojt J, Joska L and Málek J 2013 Corrosion behaviour of porous Ti–39Nb alloy for biomedical applications *Corros. Sci.* **71** 78–83
[42] Gugelmin B S, Santos L S, Ponte H A and Marino C E B 2015 Electrochemical stability and bioactivity evaluation of Ti6Al4V surface coated with thin oxide by EIS for biomedical applications *Mat. Res.* (http://dx.doi.org/10.1590/1516-1439.201514)